Int. J. Electrochem. Sci., 14 **(2019)** 33 – 43, doi: 10.20964/2019.01.13

International Journal of ELECTROCHEMICAL SCIENCE
www.electrochemsci.org

Dissolution Characteristics and Electrochemical Mechanism of NaCl-NaF-KCl-SiO_2 Melt

HuiLi[1], *JinglongLiang*[1,*], *Hongyan Yan*[1], *Yungang Li*[1], *Ramana G. Reddy*[2], *Shixian Zhang*[1], *Dongbin Wang*[1], *Jing Wang*[1]

[1]Key Laboratory of Ministry of Education for Modern Metallurgy Technology, College of Metallurgy and Energy, North China University of Science and Technology, Tangshan 063210, China
[2]Department of Metallurgical and Materials Engineering, University of Alabama, Tuscaloosa, Al 35487, U.S.A
[*]E-mail: 13373150280@163.com

Received: 4 June 2018/ *Accepted:* 26 September 2018 / *Published:* 30 November 2018

The dissolution characteristics of SiO_2 in a NaCl-KCl-NaF system were analyzed. The results showed an increase in the SiO_2 content in X_{NaCl}: X_{KCl} : X_{NaF} = 1: 1: 2, and the melt primary crystallization temperature first decreased and then increased. The temperature of primary crystallization was lowest when X_{SiO2}= 10%. The solubility of SiO_2 in the NaCl-NaF-KCl-SiO_2 melt system increases with increasing temperature. According to the thermodynamic calculations of the SiO_2-NaCl-KCl-NaF system and the XRD results, SiO_2 was dissolved in aX_{NaCl}: X_{KCl}: X_{NaF} = 1: 1: 2 melt solution at 800 °C. The surface of the deposited sample was analyzed by XRD. The intermetallic compounds Fe_3Si, FeSi and Fe_5Si_3 were generated from the dissolved Si.

Keywords: Melt; Primary crystallization temperature; Solubility; Electrochemistry

1. INTRODUCTION

Melts can provide a wider range of operating temperatures than aqueous electrolytes. Melt electro-deposition can be used to produce active metals, as well as refractory alloys and compounds, that are difficult or impossible to electrode posit from aqueous solutions. Therefore, electrolyte solutions that use melts as a solvent have received significant attention in the past 40 years[1-2]. The application of melt systems in many fields such as nuclear reactor fuels, high-energy batteries, fuel cells, energy storage and electro deposited metals has attracted a large amount of research and development. In terms of melt electrode position technology[3-5], silicon can be deposited via melts, as well as titanium[6-8] and other metals, but these species cannot be deposited using aqueous solutions[9-12]. The nature of the melt is crucial to the deposition of the metals[13]. The primary crystallization temperature also affects the

volatility of the flowing electrolyte[14] and determines the electrolysis temperature. Studying the primary crystallization temperature and solubility of the melt can provide the basis for determining the ratio of melt in the melt electro-deposition experiments and aid in the selection of the electro-deposition process conditions. It is also possible to hypothesize the chemical reactions that take place in the melt system by examining the various factors that influence the solubility, thus obtaining the melt structure. Therefore, studying the primary crystallization temperature and solubility of a melt can improve the methods for measuring the melt characteristics, promote wider development of melts and expand their application. Studying the characteristics of melts and their electrochemical reduction mechanism provides theoretical guidance for electro-deposition, and the surface properties of the deposited layer of the electro deposited sample are analyzed.

2. EXPERIMENTAL

The selected experimental compounds were pure KCl, NaCl, NaF and SiO_2. The compounds were dried in a DZF-6020-type vacuum oven, held at 200°C for 8h and then cooled naturally. The melt ratio was X_{KCl}: X_{NaCl}: X_{NaF} = 1: 1: 2, and the experimental process was carried out under an argon atmosphere.

Differential thermal analysis was conducted using a STA-449C integrated thermal analyzer with an SiO_2 mass fraction of 3%, 6%, 10% and 15%, respectively, with an empty platinum crucible as the reference crucible from room temperature to 850 °C with a heating rate of 10 °C·min^{-1}. After 10min of incubation, the temperature was reduced from 850 °C to 100 °C at the same cooling rate.

The determination of solubility was performed using a 3KL10·BYL tube furnace. The molar ratio of NaCl: KCl: NaF was 1: 1: 2, and SiO_2 was added at 2% of the total mass. The graphite crucible was placed with the compound sin to a resistance furnace for 3.5h. Then, the sample was obtained at 650, 700, 750, 800 and 850 °C, respectively, in 0.5h increments. After the melt was kept at 800°C for 4 h, the furnace was cooled to room temperature, and the melt in the upper, middle and lower layers was taken and analyzed by X-ray diffraction.

Electrochemical studies were performed using a Princeton P4000 electrochemical workstation. The electrochemical behavior of the melt was studied by cyclic voltammetry and square wave voltammetry. The working electrode was a Φ1mm iron wire; the reference electrode was a Φ0.5mm platinum wire; and the auxiliary electrode was a 2cm × 5cm × 0.2cm high-purity graphite sheet. At 800 °C, X_{KCl}: X_{NaCl}: X_{NaF} = 1:1:2, and 0.24% SiO_2 was added for electrochemical testing. The scanning range was -2.5V – 1.0V, and the scan rate was 0.9V·s^{-1}. The melt electro-deposition used a tsm-3004-type power supply, the temperature was 800 °C, the current density was 100mA·cm^{-2}, and the time was 1h. The anode was a high-purity graphite sheet (2cm × 2cm × 0.2cm) and the cathode was a silicon steel sheet (2cm × 2cm × 0.03cm) with a silicon content of 1.2%. S-4800 scanning electron microscopy was used to detect the morphology of the deposited layer. A Noran7 X-ray diffractometer was used for the phase analysis of the melt and sample.

3. RESULTS AND DISCUSSION

3.1 The primary crystallization temperature

Fig.1 showed the binary phase diagram and DTA for NaCl-KC-NaF. According to the principle of differential thermal analysis, the first peak on the left in Figure (b) indicates the complete solidification temperature, and the second peak indicates the primary crystallization temperature. The NaCl-KCl-NaF melt primary crystallization temperature was 783.7 °C, and the complete solidification temperature was 600.6 °C, which is consistent with the primary crystallization temperature region in the phase diagram was shown in Fig. 1 (a).

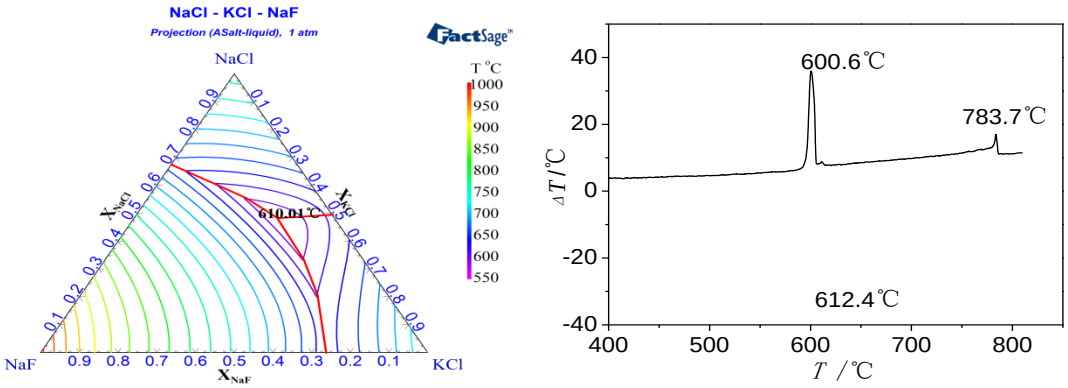

Figure 1. Binary phase diagram and DTA for NaCl-KC-NaF(X_{KCl}:X_{NaCl}:X_{NaF} = 1:1:2)

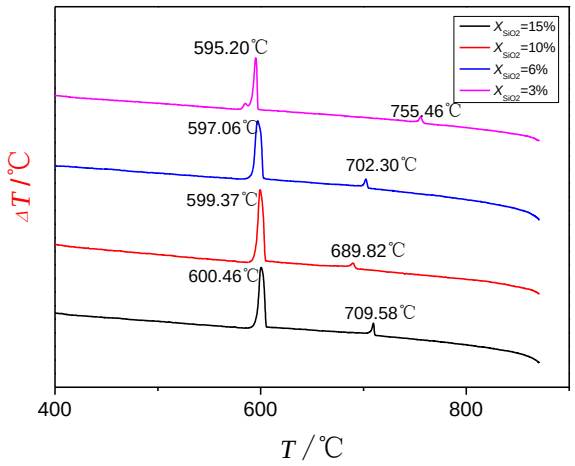

Figure 2. Effect of SiO_2 on the primary crystallization temperature of the NaCl-KC-NaF melt (X_{KCl}: X_{NaCl}: X_{NaF} = 1: 1: 2)

As shown in Fig.2, in order to study the influence of the SiO_2 content on the primary crystallization temperature of the NaCl-KCl-NaF melt system, differential thermal analysis of the melt system with different mass fractions of SiO_2 was carried out. Compared with Fig.1(b), the SiO_2 content had a great influence on the primary crystallization temperature of the NaCl-KCl-NaF melt system and had little influence on the complete solidification temperature. This was because the primary crystal

temperature was mainly affected by atomic interactions and molecular interactions. The addition of SiO_2 to the NaCl-KCl-NaF melt reduces the intermolecular interactions of the original melt, thus reducing the primary crystal temperature[15]. The primary crystallization temperature of the NaCl-KCl-NaF melt system first decreased and then increased with an increasing SiO_2 content. When X_{SiO2}<10%, the primary crystallization temperature of the melt decreases with increasing SiO_2. When X_{SiO2}>10%, the primary crystallization temperature of the melt increases with increasing SiO_2. That because the content of SiO_2 was in the range of 3% ~ 15%. This range covered the content of SiO_2 at the eutectic point. When the SiO_2 was close to the eutectic point, the lowest point temperature was achieved. Therefore, when the SiO_2 content was in range between 3% ~ 15%, the primary crystallization temperature first decreases and then increased with increasing SiO_2[16].

3.2 The solubility of SiO2 in the NaCl-NaF-KCl melt

As shown in Fig.3, the amount of dissolved SiO_2 at different temperatures was measured in the NaCl-NaF-KCl-SiO_2 melt. Fig.3 (a) shows that, at constant temperature, the dissolved amount of SiO_2 gradually increases with increasing holding time. When the temperature was between 650–700 °C, the amount of dissolved SiO_2 had a linear relationship with the holding time. When the temperature increases to 800°C, the effect of holding time on the dissolution of SiO_2 was obviously enhanced. The relationship between the dissolution of SiO_2 and the holding time deviates from the linear relationship, and the amount of dissolved SiO_2 gradually increased as the holding time was extended until gradually reaching an equilibrium after a certain time. This was because as the reaction progresses, the forward reaction rate gradually decreases and the reverse reaction rate gradually increased until the forward and reverse reaction rates were equal and no longer change, meaning the reaction reached equilibrium. As the temperature raised, the time required for the reaction to reach equilibrium decreases. Because as the temperature increased, the molecular motion accelerated and increased the number of collisions. In addition, the molecules gain energy, and the number of molecules that reach the activation energy increased, the reaction rate was accelerated, and the time required for the reaction to reach equilibrium was reduced.

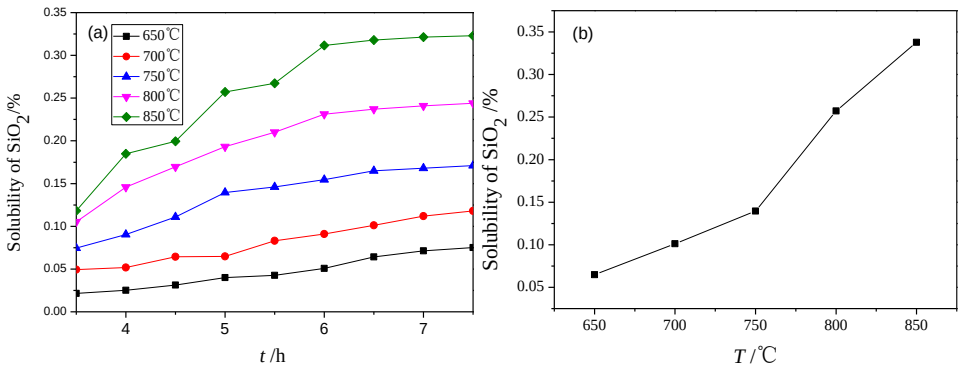

Figure 3. The dependence of SiO_2 content in the NaCl-NaF-KCl-SiO_2 melt on time at 650℃-850℃.

In the NaCl-NaF-KCl-SiO_2 melt system, the dissolution of SiO_2 increased with increasing temperature. At 650–750°C, the effect of temperature on the dissolution of SiO_2 was small. At 750–

850°C, the effect of temperature on the dissolution of SiO_2 was obvious, and the dissolution of SiO_2 increased rapidly. When the temperature raised, ion migration and molecular diffusion rate up, the ions in the crystal lattice heated up, and the energy increased and tend to leave the crystal lattice, making the crystal lattice more unstable. At the same time, the energy of the solvent molecules became higher and the molecular motion accelerated, increasing the effective number of times the solvent molecules attack the lattice. As a result, the lattice was more easily destroyed. At the same time, increasing the temperature reduces the density of the melt[17], loosens the ionic group structure, reduced the interactions between the anionic compounds and cationic compounds, and increased the ion diffusion coefficient and "micro-pore structure" [18] of the melt, which was in favor of SiO_2 dissolution. The rate of ion migration and molecular diffusion was accelerated, and SiO_2 continues to dissolve. Because SiO_2 was in a supersaturated state, the high temperature increases the amount of dissolved SiO_2. At low temperature, ion migration and molecular diffusion were slow and SiO_2 dissolves less. With increasing temperature, SiO_2 dissolved more slowly.

3.3 Thermodynamic calculations

The experimental conditions were above 800 °C, and the reactants were SiO_2, NaCl, KCl and NaF. Because of the similar nature of KCl and NaCl, there are five combinations of SiO_2 + NaCl, SiO_2 + NaF, SiO_2 + NaCl + NaF, SiO_2 + KCl and SiO_2 + KCl + NaF. After HSC software analysis and calculations, the possible reaction equations could be divided into valence changes and non-valence changes[19].

The first type of redox reaction:

$$6KCl+3SiO_2+NaCl=KClO_3+3SiCl_2(g)+3Na_2SiO_3 \quad (1)$$

$$KCl+3SiO_2+6NaCl=KClO_3+3SiCl_2(g)+3Na_2O \quad (2)$$

$$6KCl+3SiO_2+NaCl=NaClO_3+3SiCl_2(g)+3K_2O \quad (3)$$

$$KCl+4SiO_2+8NaCl=KClO_4+4SiCl_2(g)+4Na_2O \quad (4)$$

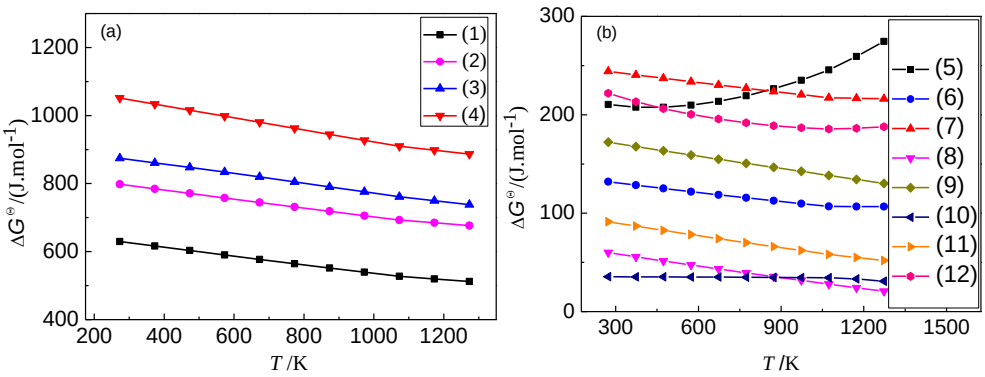

Figure 4. Variation of ΔG^{θ} versus temperature from 0–1000 °C, ΔG^{θ} of the mutual reactions among substances in melt

The second type of equation:

$$12NaF+9SiO_2+4KCl=6Na_2SiO_3+2K_2SiF_6+SiCl_4(g) \quad (5)$$

$$3SiO_2(l)+4NaCl(l)=2Na_2SiO_3(l)+SiCl_4(g) \quad (6)$$

$$SiO_2(l)+4NaCl(l)=2Na_2O(l)+SiCl_4(g) \quad (7)$$

$$3SiO_2+4NaF=2Na_2SiO_3+SiF_4(g) \quad (8)$$

$$SiO_2+4NaF=2Na_2O+SiF_4(g) \quad (9)$$

$$3SiO_2+6NaF=Na_2SiF_6+2Na_2SiO_3 \quad (10)$$

$$3SiO_2+3NaF+NaCl=SiClF_3(g)+2Na_2SiO_3 \quad (11)$$

$$9SiO_2+12NaF+2KCl=2SiClF_3(g)+6Na_2SiO_3+K_2SiF_6 \quad (12)$$

Using the equations, the standard Gibbs free energy curve (ΔG^{θ}) *vs.* temperature in the experimental temperature range were shown in Fig. 4. At 800 °C, the standard Gibbs free energy for Equations (1) to (12) was positive, $\Delta G^{\theta} > 0$. This means none of the above reactions spontaneously proceed under these experimental conditions. However, it was generally considered that when $|\Delta G^{\theta}| < 41.8 kJ \cdot mol^{-1}$, the sign of ΔG^{θ} cannot determine the sign of ΔG, so it was difficult to judge the direction in which the reaction proceeds. Over the experimental temperature range, the standard Gibbs free energies of equations (8) and (10) was less than $41.8 kJ \cdot mol^{-1}$, $|\Delta G^{\theta}| < 41.8 kJ \cdot mol^{-1}$.

3.4. Melt XRD analysis

The NaCl-KCl-NaF melt with an SiO_2 mass fraction of 3% was heated to a temperature of 800°C and kept at that temperature for 4.5 h. The upper, middle and lower melts were taken for X-ray diffraction analysis, as shown in Fig. 5. The upper, middle and lower layers of the melt contain unreacted NaF, KCl and NaF, and both contained the product Na_2SiO_3. Combined with the standard Gibbs free energy, both equations (8) and (10) are possible, and no new Na_2SiF_4 material was found in the upper and middle layers of the melt. At 800 °C, the Gibbs free energy of (8) is lower, and the reaction is more likely to occur. In addition, the upper and middle melts have newly formed Na_2SiO_3 material, and SiO_2 was not found. Under the experimental conditions, when dissolved in melt,SiO_2 and NaF undergo a chemical reaction to form a new material —Na_2SiO_3. The lower melt of NaCl, KCl, SiO_2 and NaF indicate that under the experimental conditions, the melt is still part of the added SiO_2 that did not dissolve and is deposited at the bottom in a supersaturated state. Therefore, the chemical dissolution of SiO_2 in the NaCl-KCl-NaF melt system could be confirmed by the thermodynamic calculations and X-ray diffraction analysis.

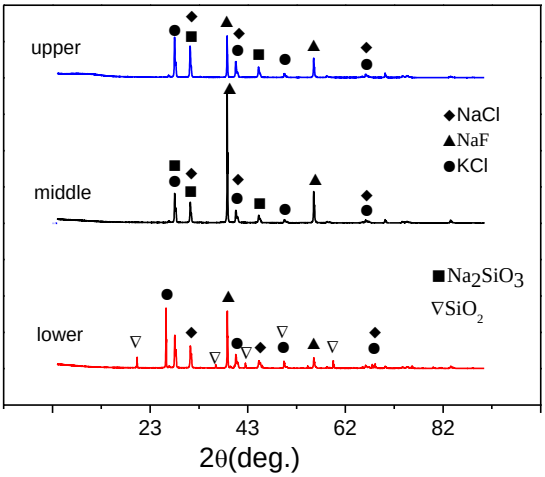

Figure 5. X-ray diffraction pattern of the melt. The NaCl-KCl-NaF melt with a SiO_2 mass fraction of 3% was heated to a temperature of 800 °C and maintained for 4.5 h.

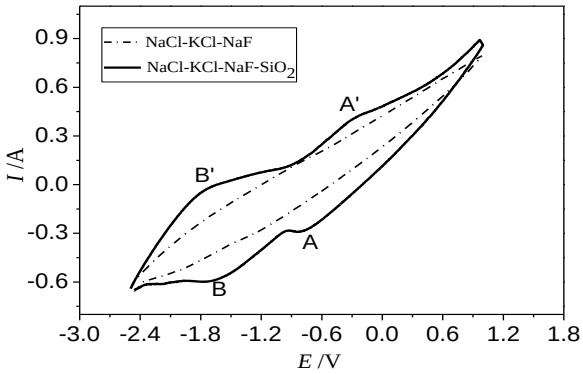

Figure 6. Cyclic voltammograms of NaCl-NaF-KCl in the melt with and without 0.24% SiO_2. Scan rate: $0.9V \cdot s^{-1}$.

3.5 Electrochemical reduction mechanism

3.5.1 Cyclic voltammetry

The inexpensive alkali metal and alkaline earth metal chloride salts have a low melting point, a wide electrochemical window and good electrical conductivity, and were suitable melts for the direct preparation of metallic silicon and its compounds[20-23]. The NaCl-NaF-KCl and NaCl-NaF-KCl-SiO_2 melt systems were analyzed by cyclic voltammetry, and the results were shown in Fig. 6. The cyclic voltammetry curve of the blank salt NaCl-NaF-KCl was shown in the dotted line in Fig. 6. There were no redox reactions occurred in the scanning potential range -2.5V~1.0V. The solid line in Figure 6 was the cyclic voltammetry after the addition of SiO_2. Due to the faster scan rate, a significant redox peak could be seen in the scanning potential range -2.5V~1.0V. When scanning in the forward direction, B' corresponded to the oxidation of sodium, and A' corresponded to the oxidation of silicon. When scanning in the backward direction, two obvious reduction peaks A(-0.8 V) and B(-1.7 V) appeared in the NaCl-

NaF-KCl-SiO_2 melt system. Theoretically, the precipitation potential of Si in the chloride system was more positive than the precipitation potential of Na. Therefore, peaks A and B correspond to the reduction of Si(IV). Peak A corresponding step-by-step reduction reaction: Si(IV)+2e=Si(Ⅱ)[24]. Peak B corresponding step-by-step reduction reaction: Si(Ⅱ)+2e=Si. Jia[25] et al also pointed out that the deposition of silicon was obtained from Si(II) + 2e = Si in the Na_3AlF_6-LiF melt system. These results suggest that Si(IV) was deposited and reduced on the Fe electrode through a two-step electron transfer process. This was consistent with the results reported by Haarberg[26] et al. Through the electrochemical deposition of Si on Ag, W and glassy carbon electrodes, it was concluded that the deposition and reduction of silicon in a KF-LiF-K_2SiF_6 melt is a two-step process. In this work, the results also demonstrate that the deposition of silicon is a two-step process.

3.5.2 Square-wave voltammetry

The square-wave voltammetry curve of a Fe electrode in the NaCl-NaF-KCl-SiO_2 melt was measured by square-wave voltammetry. As shown in Fig.7, two obvious reduction peaks A (-0.8V) and B (-1.7V) appear in the curve, and the peaks correspond to a two-step reduction of Si(IV) on the Fe electrode. The electron transfer number (n) of Si(IV) was calculated from the half-value width ($W_{1/2}$) formula[27]:

$$W_{1/2}=3.52RT/nF \quad (13)$$

According to the square-wave voltammogram, the $W_{1/2}$ value of peak A was 0.18V, and the $W_{1/2}$ value of peak B was 0.22V. Using formula (13), the number of electrons transferred by the reduction peak A was n = 1.9, which was approximately equal to 2; the number of electrons transferred by the reduction peak B was n = 1.5, which also equals approximately 2. Therefore, it was determined that the reaction of Si(IV) on the Fe electrode corresponding to the reduction peaks A and B were:

$$Si(IV)+2e=Si(II)$$

$$Si(II)+2e=Si$$

These results were consistent with in the cyclic voltammograms.

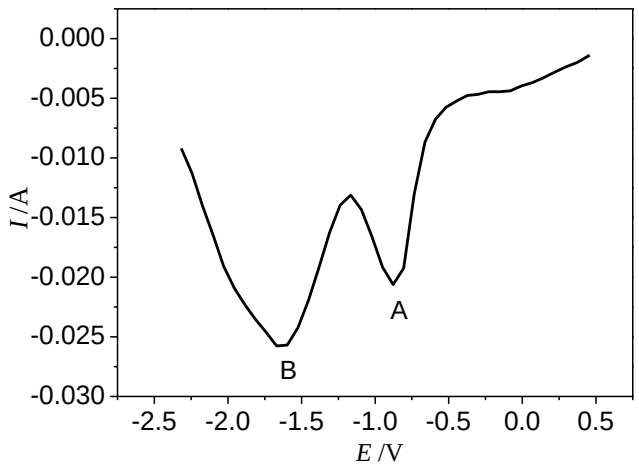

Figure 7. Square-wave voltammetry on Fe electrodes in NaCl-NaF-KCl-0.24%SiO_2 melt

3.6. Characterization of Deposited Films in Melt

For electro-deposition, atemperature of 800 °C was selected with a time of 1h in the NaCl-KCl-NaF-SiO_2 melt system. The results of the deposited surface morphology and content of the sample, as well as the surface phase analysis, were shown in Figure 8.

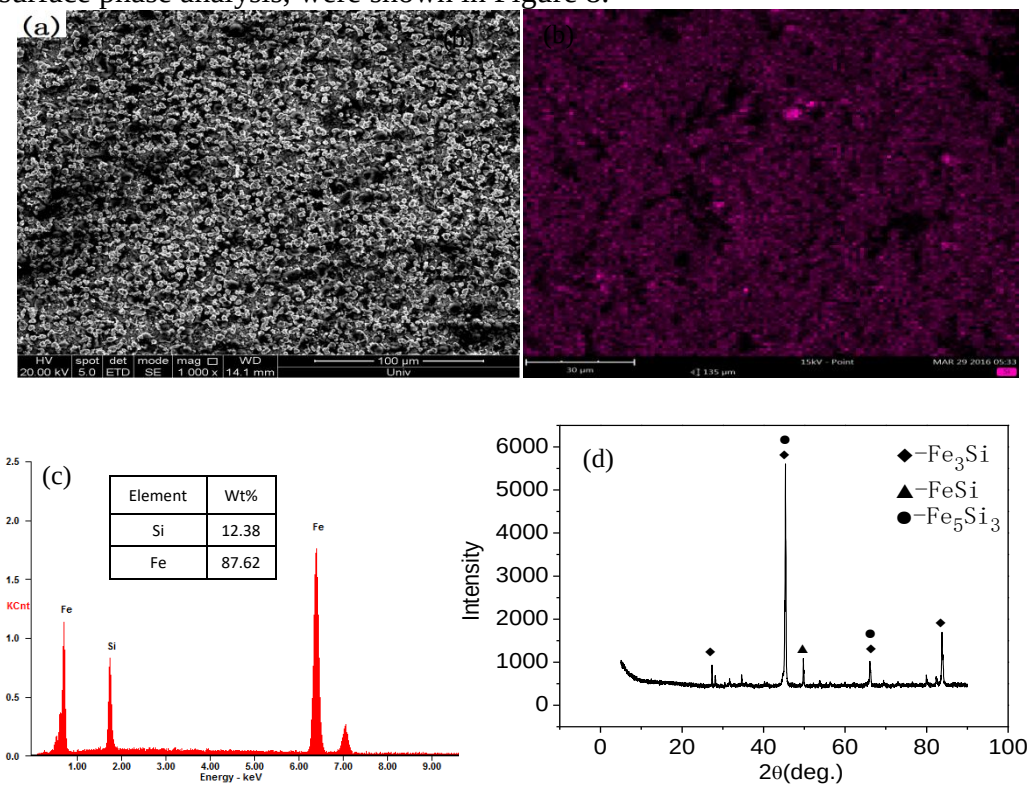

Figure 8. The surface morphology EDS and XRD mapping analysis of the sample after deposition for 1h at 800 °C(a) SEM, (b) Silicon surface scan, (c) EDS, and (d) XRD

As shown in Fig. 8, the surface of the deposited layer was evenly distributed. As shown in Fig.8(b) and (c), the mass fraction of Si on the sample surface was 12.38%, and the Si was uniformly distributed on the surface of the Fe-Si alloy. The Fe atom covalent radius is 1.17 and the Si atomic covalent radius is 1.11, both of which are close to each other. It was impossible to form a gap in a solid solution. Therefore, Si undergoes displacement diffusion in the Fe-Si alloy, and there was a very low equilibrium concentration of interstitial atoms. Hence, the contribution of the interstitial mechanism in diffusion was negligible. So the vacancy mechanism and exchange mechanism correspond to the diffused forms of Si in the Fe-Si alloys. As shown in Fig. 8 (d), the intermetallic compounds Fe_3Si, FeSi and Fe_5Si_3 were presented on the surface of the deposited layer. According to the Fe-Si binary phase diagram[28]，there are many phase structures in Fe-Si binary phase diagrams, including Fe_3Si, FeSi, Fe_5Si_3 and Si atoms dissolved in the interstitial spaces of Fe atoms to form ordered solid solutions. This indicated that the amount of silicon was at least 0.75kmol, which means the surface silicon content was at least 11%, as when the content of silicon was less than 1.6%, there were only Fe and Fe_3Si phases in the system. When the silicon content reached to 1.6–11%, there were Fe, Fe_3Si and FeSi phases in the

system. When the silicon content reached to 11–33%, the amount of silicon was 0.75kmol, and the phases in the system were Fe, Fe_3Si, FeSi and Fe_5Si_3[29]. Therefore, Fe_3Si, FeSi and Fe_5Si_3 were presented on the surface of the sample electro-deposited for 1h at 800°C.

4. CONCLUSIONS

The primary crystal temperature, solubility and structure of the melt are important properties in melt electro-deposition and were related to the smooth progress of melt electro-deposition. Therefore, studying the characteristics of a melt could lay a theoretical foundation for the electro-deposition process. Electrochemical analysis was used to study the cathodic reduction mechanism during the electro-deposition process, and the surface deposition of the electro-deposited sample was analyzed. The conclusions were as follows:

(1) In the melt of X_{NaCl}:X_{KCl}:X_{NaF}=1:1:2, when the content of SiO_2 was increased, the primary crystallization temperature first decreased and then increased. When, X_{SiO2} was 10%, the primary crystallization temperature reached its minimum.

(2) In an NaCl-NaF-KCl-SiO_2 melt system, the solubility of SiO_2 increased with increasing temperature.

(3) The dissolution of SiO_2 in the NaCl-KCl-NaF melt system was chemical dissolution.

(4) The reduction of Si(IV) on the Fe electrode was a two-step electronic process. That should be ascribed to the consecutive reduction reactions o f Si(IV)→Si(II)→Si(0.).

(5) According to the analysis of the surface scan results, the silicon was uniformly distributed in the Fe-Si alloy, and the XRD patterns showed that the intermetallic compounds Fe_3Si, FeSi and Fe_5Si_3 were formed from Fe and Si.

ACKNOWLEDGEMENTS
This study was financially supported by the National Natural Science Foundation of China (Project Nos. 51674120, 51474093), the Natural Science Foundation of Hebei Province (Project No. E2016209163) and the high school science and technology (Project No.BJ2017050).

References

1. Y. Gu, J. Liu, S. Qu, Y. Deng, X. Han and W. Hu, *J. Alloy Compd*., 690 (2017) 228.
2. R.Abdulaziz, L.D. Brown, D. Inman, P.R. Shearing and D.J.L. Bret, *Electrochim. Acta*, 226 (201 7)18.
3. Y.D. Yan, M.L. Zhang, X.Y,H. Wei, D.X. Cao and S.Q. Wei, *Electrochim. Acta*, 54 (2009) 3387.
4. W. Han, M. Li, M.L. Zhangand Y.D. Yan, *Rare Metals*, 35(2016)811.
5. M. Fukumoto, Y. Aiand M. Hara, *Oxid. Met.*, 85(2016)17.
6. P. Ozkalafat, G.K. SireliandS. Timur, *Surf. Coat.Tech.*, 308 (2016) 128.
7. Q.G. Weng, R.D. Li, T.C. Yuan, J. Li and Y.H. He, *T.Nonferr. Metal. Soc.*, 24(2014) 553.
8. A.A. Shevyrev and V.N.Kolosov, *Inorg. Mater+*. , 47(2011)29.
9. G.M. Haarberg, L.Famiyeh, A.M. Martinez and K.S. Osen, *Electrochim. Acta*, 100 (2013) 226.

10. A.L. Bieber, L. Massot, M. Gibilaro, L. Cassayre, P. Taxil and P. Chamelot, *Electrochim. Acta*, 62 (2012) 282.
11. A.L. Bieber, L. Massot, M. Gibilaro, L. Cassayre, P. Chamelot and P. Taxil., *Supplemental Procee dings: Mater. Process.Energ. Mater.*, 1 (2011)723.
12. S.Zhuk, V. Isaev, O. Grishenkova, A. Isakov, A. Apisarov and Y. Zaykov, *J. Serb. Chem. Soc.*, 82 (2016) 51.
13. Y. Sakanaka, A. Murata, T. Gotoand K. Hachiya, *J.Alloy. Compd*., 695 (2017) 2131.
14. S.Wang,H. Luo, H. Deng, S. Xiao and W. Hu, *J. Mol.Liq.*, 234 (2017) 220.
15. Z.Y. Xie, Z. Wangand Y. Han, *J Alloy. Compd.*, 672 (2016) 332.
16. Y.G. Li,Shenyang: Northeastern University, 2005.
17. M.G. Bao, Z.W. Wang, B.L. Gao, Z.N. Shi, X.W. Hu and J.Y. Yu, *Adv. Mater. Res.*, 968 (2014) 6 7.
18. X.W. Hu, Z.W. Wang, B.L. Gao, Z.N. Shi, F.G. Liu and X.z. Cao, *J. Rare Earth*., 28 (2010) 587.
19. J. Pourasad and N. Ehsani, *Int. J. Mater. Res.*, 107 (2016) 1026.
20. S.L. Wang, S.C. Li, S.H. Cao, *Int. J. Miner. Metall. Mater*. 17 (2010) 791.
21. E.B. Freidina, D.J. Fray, *Thermochim. Acta*, 354 (2000) 59.
22. R.O. Suzuki, K. Teranuma, K. Ona, *Metall. Mater. Trans. B Process Metall. Mater. Process. Sci.*, 34 (2003) 287.
23. W. Weng, M.Y. Wang, X.Z. Gong, Z. Wang, Z.C. Guo, *Chin. J. Chem. Eng.*, 24 (2016) 671.
24. R. Boen, J. Bouteillon, *J. Appl. Electrochem*., 13(1983) 277.
25. M. Jia, Y.Q. Lai, Z.L. Tian, F.Y. Liu, J. Li, P.F. Xin and Y.X. Liu, *Acta. Phys.-Chin. Sin*., 27(2011)1108.
26. G.M. Haarbery, L. Famiyeh, A.M. Martinez and K.S. Osen, *Electrochim. Acta*, 100 (2013)226.
27. C.Hamel,P.Chamelot, A.Laplace,E. Walle, O. Dugne and P. Taxil, *Electrochim. Acta*,52(2007)399 5.
28. H. Meco and R.E. Napolitano, *Scripta Mater*., 52 (2005) 221.
29. Y.Y. Li, J.L. Liang.Z. Tang and W. Tian, *Chin. J. Nonferr. Met.*, 19(2009)714.

© 2019 The Authors. Published by ESG (www.electrochemsci.org). This article is an open access article distributed under the terms and conditions of the Creative Commons Attribution license (http://creativecommons.org/licenses/by/4.0/).